

**UV Spectroscopy of AB Doradus with the Hubble Space
Telescope.¹**

**Impulsive flares and bimodal profiles of
the CIV 1549 line in a young star**

O. Vilhu²

NORDITA, Blegdamsvej 17, DK-2100 Copenhagen, Denmark, and Observatory, Box 14,
FIN-00014 University of Helsinki, Finland

Electronic mail: osmi.vilhu@helsinki.fi

P. Muhli, J. Huovelin and P. Hakala

Observatory, P.O. Box 14, FIN-00014 University of Helsinki, Finland

Electronic mail: muhli@gstar.astro.helsinki.fi, huovelin@fornax.astro.helsinki.fi,
pahakala@sirius.astro.helsinki.fi

S.M. Rucinski

David Dunlap Observatory, University of Toronto, P.O. Box 360 Richmond Hill, Ontario,
Canada LYC 4YC

Electronic mail: rucinski@astro.utoronto.ca

and

A. Collier Cameron

School of Physics and Astronomy, University of St Andrews, North Haugh, St Andrews,
Five, Scotland KY16 9SS

Electronic mail: acc4@st-andrews.ac.uk

Received _____; accepted _____

¹Based on observations with the NASA/ESA *Hubble Space Telescope*, obtained at the Space Telescope Science Institute which is operated by the Association of Universities for Research in Astronomy, Inc., under NASA Contract NAS5-26555.

²*Hubble Space Telescope* Guest Observer

ABSTRACT

We observed AB Doradus, a young and active late type star (K0 - K2 IV-V, $P = 0.514$ d) with the Goddard High Resolution Spectrograph of the post-COSTAR *Hubble Space Telescope* with the time and spectral resolutions of 27 s and 15 km s^{-1} , respectively (November 14.08 - 14.30, 1994 (UT)). The wavelength band (1531 - 1565 Å) included the strong CIV doublet (1548.202 and 1550.774 Å, formed in the transition region at 10^5 K), the chromospheric SiII 1533.432 Å line and the blend of SiI, CI and FeII lines at 1561 Å. The mean quiescent CIV flux state was characterized by $F_{CIV} = (7.80 \pm 0.34) \times 10^5 \text{ ergs cm}^{-2} \text{ s}^{-1}$, close to the saturated value and 100 times the solar one. The line profile (after removing the rotational and instrumental profiles) is bimodal consisting of two Gaussians, narrow (FWHM = 70 km s^{-1}) and broad (FWHM = 330 km s^{-1}). This bimodality is probably due to two separate broadening mechanisms and velocity fields at the coronal base. It is possible that TR transient events (random multiple velocities), with a large surface coverage, give rise to the broadening of the narrow component, while true microflaring is responsible for the broad one as suggested by Wood, Linsky and Ayres (1997).

The transition region was observed to flare frequently on different time scales and magnitudes. The largest impulsive flare seen in the CIV 1549 Å emission at day 14.22 reached in less than one minute the peak differential emission measure $N_e^2 V (10^{4.85} \text{ K} - 10^{5.15} \text{ K}) = 10^{51.2} \text{ cm}^{-3}$ and returned exponentially in 5 minutes to the 7 times lower quiescent level. The 3 min average line profile of the flare was blue-shifted (-190 km s^{-1}) and broadened (FWHM = 800 km s^{-1}). This impulsive flare could have been due to a chromospheric heating and subsequent evaporation by an electron beam, accelerated (by reconnection) at the apex of a coronal loop.

1. Introduction

AB Doradus (HD 36705) is one of the most interesting active late-type stars observed from radio to X-rays. It has short rotation period (0.514 d), small age 10^{7-8} yr and spectral type K0-K2 IV-V (for some recent works see e.g. Vilhu *et al.* 1993; Rucinski *et al.* 1995; White *et al.* 1996). The new distance 15 pc is based on the combined HIPPARCOS data and VLBI radio techniques giving a parallax 0.0663-0.0672 arc sec (Guirado *et al.* 1997). These astrometric observations also discovered another low mass companion (around 0.1 solar masses) of AB Dor at separation of 0.2-0.7 arc sec, in addition to the known visual companion Rst137B at 10 arc sec.

Striking features are the frequently observed X-ray flares (twice/day, see Vilhu *et al.* 1993), and the persistent (over 15 years) photometric ephemeris, explained by spots at active longitudes (Innis *et al.* 1988):

$$\text{PHASE} = 0.0 : \text{HJD} = 2444296.575 + 0.51479\text{E} \quad (1)$$

An interesting discovery were the prominence-like condensations trapped in corotation at several stellar radii above the surface (Cameron & Robinson 1989). At least a part of the stellar angular momentum loss takes place through these clouds.

Many studies have demonstrated the usefulness of the strong CIV 1549 Å doublet (formed at the transition region) for studying the magnetic activity (dynamo power) in solar-type stars. The emission saturates at around $F_{\text{CIV}}/F_{\text{BOL}} = 2.5 \times 10^{-5}$ (Vilhu 1987). One of the major discoveries of the GHRS (Goddard High Resolution Spectrograph) on board the *Hubble Space Telescope* has been the detection of bimodal structures and broad wings of the CIV 1549 lines in some active cool stars. Linsky & Wood (1994) were the first to report broad CIV and SiIV line profiles in the flare star AU Mic (dM0), even during

the quiescent state. They fitted the quiescent spectrum of AU Mic by two components with relative fluxes $F_B/F_N = 0.58$ and $\text{FWHM}_B/\text{FWHM}_N = 173 \text{ km s}^{-1}/29 \text{ km s}^{-1}$. The quiescent CIV flux was high ($6.3 \times 10^5 \text{ ergs cm}^{-2} \text{ s}^{-1}$), somewhat higher than the ‘maximum saturated’ value at M0 ($2 \times 10^5 \text{ ergs cm}^{-2} \text{ s}^{-1}$).

The second example, Capella (a binary star, G1 III + G8 III), was observed by Linsky *et al.* (1995). The G1-star ($v \sin i = 36 \text{ km s}^{-1}$) contributes 88 % of the CIV flux from the system, and is composed of a moderately broad ($\text{FWHM} = 164 \text{ km s}^{-1}$) and a very broad component ($\text{FWHM} = 360 \text{ km s}^{-1}$), with flux ratios around 0.8. The mean surface flux of the G1-component was roughly $F_{\text{CIV}} = 1.5 \times 10^5 \text{ ergs cm}^{-2} \text{ s}^{-1}$, which is 10 times lower than the saturated value at this spectral type, but still higher than that of a solar plage ($10^{4.5-5.0} \text{ ergs cm}^{-2} \text{ s}^{-1}$). Linsky *et al.* proposed that the very broad wings of the transition region lines of Capella are due to stellar analogs of solar transition region explosive events (Brueckner *et al.* 1988, Dere *et al.* 1989). Wood *et al.* (1996) analyzed the GHRS observations of HR 1099 and found one more example of very broad wings in the transition region lines.

Later, the number of stars observed has increased. At present, the most comprehensive collection of broad wings is in the important paper by Wood, Linsky and Ayres (1997), including 12 stars with different activity levels and spectral and luminosity classes (including the measurements of AB Dor of the present paper). In particular, it was shown that the contribution of the broad component correlates with activity indicators like the X-ray surface flux.

Preliminary results of the present study were reported by Vilhu *et al.* (1996). In the present paper we describe these observations of AB Doradus in a more detail.

2. Observations

The observations (see Table 1) covered November 14.08 - 14.30, 1994 (UT) corresponding to rotational phases between 0.21 - 0.64 (Eq. 1). The observations were carried out during the Continuous Viewing Zone (CVZ), with no interrupted sequences owing to Earth occultations. The post-COSTAR GHRS (cycle 4) was used with the medium resolution grating G160M, centered at the CIV 1550 doublet, giving resolving power of 20000 (see GHRS Instrument Handbook). The ACCUM mode with STEP-PATT = 5 gave time resolution of 27 s.

The wavelength coverage was 1531 - 1565 Å with a diode spacing in the substep pattern of 0.019 Å (3.7 km s⁻¹). In addition to the strong CIV 1548.202 and CIV 1550.774 lines (the optically thin theoretical ratio of which equals to 2), the region contains also the well visible chromospheric SiII 1533.432 line and the broad blend at 1560 Å, consisting of chromospheric SiI, CI and FeII lines (see Fig. 1).

The instrumental profile was Gaussian with a FWHM approximately 15 km s⁻¹. The wavelength calibration was based on the exposure of the calibration lamp just before the observing run. The magnetic anomalies (GIMP) were estimated (by D. Soderblom, from the model hrs-gimp which uses spacecraft position) and their effect on the wavelength scale was found small (less than ± 0.01 Å), although occasionally it could reach a quarter of a diode (0.019 Å = 3.7 km/s). Further, the temperature corrections applied by the calhrs-routine has been generally good, leading to no significant zero-point nor dispersion error (D. Soderblom, private comm.)

The strong CIV doublet (quiescent flux $\sim 1.0 \times 10^{-12}$ ergs cm⁻² s⁻¹, see Table 2) is contaminated by weak chromospheric SiI lines (at 1548.978, 1551.240, 1551.454 and 1551.856 Å). However, their effect is very small and can be neglected because in active stars the transition region lines are much more enhanced than the chromospheric ones. In solar

plages, resembling the outer atmospheres of moderately active stars, these lines comprise 4 % of the CIV line fluxes. In the extremely active AB Dor we can expect this percentage to be still lower. The weaknesses of the SiII 1533.432 line (1.8×10^{-14} ergs cm⁻² s⁻¹) and the 1560-blend (7.1×10^{-14} ergs cm⁻² s⁻¹) also confirm this: in the quiet sun and solar plages these lines are stronger than the SiI lines inside the CIV-profile (Fig. 1).

EDITOR: PLACE TABLE 1 HERE.

EDITOR: PLACE FIGURE 1 HERE.

The single SiII 1533.432 line (see Fig. 1) can be well fitted with the 90 km s⁻¹ rotational and 15 km s⁻¹ instrumental profiles. Hence, these (previously known) broadening values are also used in the present paper.

A photospheric dark spot (the spot 'B' at phase 0.5, defined by Innis et al. 1988) was well visible during our observations, causing the minimum in the simultaneous ground-based optical U-band light curve (Fig. 2, Las Campanas/University of Toronto 61 cm telescope).

EDITOR: PLACE FIGURE 2 HERE.

EDITOR: PLACE FIGURE 3 HERE.

EDITOR: PLACE FIGURE 4 HERE.

EDITOR: PLACE TABLE 2 HERE.

EDITOR: PLACE TABLE 3 HERE.

Figures 3 and 4 show the time-evolution of the CIV line during the observations (5.4 hours). Especially remarkable are the impulsive flares (see the next section).

3. Impulsive Flaring

A striking feature of the CIV line is the frequent flaring (Fig. 3 and 4). The line intensity is variable on different time scales: AB Dor spends approximately 15 % of the time above the $+3\sigma$ level from the mean quiescent state, defined as the CIV flux-level averaged over the rotational phases 0.25-0.35 and 0.50-0.60 without significant flares. On the other hand, the flares were not detected in the far UV continuum close to CIV 1550 (these observations) and in the optical U-band continuum (see Fig. 2). In addition, the flux of the nearby chromospheric lines did not increase during the flares at all. These constant lines were the single SiII 1533.432 line, and the blend of SiI, CI and FeII lines at 1561 Å.

The CIV light curves around the two strongest flares at day 14.185 and 14.22 were fitted with an exponential function which has also been used for modelling of the temporal behaviour of Gamma Ray Bursts (see Norris *et al.* 1994):

$$F(t) = A \exp[-(|t - t_{max}|/\sigma_{r,d})^\nu] + B, \quad (2)$$

where A denotes the maximum intensity of the flare relative to the quiescent intensity B , and t_{max} is the corresponding time coordinate. σ_r and σ_d are the rise ($t < t_{max}$) and decay ($t > t_{max}$) times of the flare, respectively, and ν is the flare “peakedness”. A least squares fit was applied to the CIV light curve between day fractions 14.173 - 14.196 and 14.207 - 14.230 (corresponding to rotation phase intervals of 0.394-0.406 and 0.462-0.474,

respectively), yielding the following results for the day 14.185 and 14.22 flares, respectively (errors are 1σ): $A = 1.93 \pm 0.17$ and 7.18 ± 0.93 ergs $\text{cm}^{-2} \text{s}^{-1}$, $B = 1.52 \pm 0.04$ and 1.20 ± 0.04 ergs $\text{cm}^{-2} \text{s}^{-1}$, $t_{max} = 14.1837 \pm 0.0002$ and 14.2179 ± 0.0000 UT, $\sigma_r = 115 \pm 24$ and 26 ± 4 seconds, $\sigma_d = 229 \pm 30$ and 96 ± 17 seconds, $\nu = 1.90 \pm 0.42$ and 0.94 ± 0.14 . The CIV light curves and the corresponding fits are shown in Figs. 5a and 5b.

EDITOR: PLACE FIGURE 5 HERE.

The strongest flare (rise time 26 s, decay time 96 s) at day 14.22 is well represented (3 min mean) by the quiescent profile *plus* a very broad (FWHM = 800 km s^{-1}) and blue-shifted (-190 km s^{-1}) Gaussian profile (see Fig. 6 and Table 3). This impulsive flare deserves a special discussion. The error estimate of its rise time ($26 \pm 4\text{s}$) is probably too optimistic and formal given by the fitting method (see Table 2). However, the rise time can in principle be determined with a better accuracy than the time resolution (like the wavelength can often be measured more accurately than the spectral resolution). The result is, however, marked by (:) in the Table 2.

During the flare (and during the whole observing run) the line ratio CIV1548/CIV1551 remained constant (around 1.9), close to the theoretical non-saturated value 2.0. This indicates that the flaring plasma remained effectively thin (the line photons once created escape from the region after perhaps many scatterings). The narrow (FWHM = 55 km s^{-1}) and slightly blue-shifted (-50 km s^{-1}) absorptions seen during the flare (see Fig. 6) had approximate equivalent widths 0.3 Å and 0.2 Å, respectively (after the quiescent component was subtracted). This would mean that the flaring upwards moving plasma became somewhat optically thick (although remaining effectively thin), or alternatively the absorptions were caused by some unlucky short-term instrumental effect (like intermittent diodes). This last possibility is unlikely because it is seen in both line components (see

Fig.6).

A solar flare with similar time-evolution was observed by Brekke *et al.* (1996) with the Solar-Stellar Irradiance Comparison Experiment (SOLSTICE). The rise time of that flare was 10 s and it decayed in a few minutes. The peak intensity of CIV 1549 emission reached around 12.5 times the pre-flare value (Brekke et al., their Table 2). In AB Dor the flare peak CIV-flux reached 6.6 times its quiet value $7.8 \times 10^5 \text{ ergs cm}^{-2} \text{ s}^{-1}$. Using for the quiet sun a surface flux of $10^{3.7-4.0} \text{ ergs cm}^{-2} \text{ s}^{-1}$, and assuming that the radii of the sun and AB Dor are comparable, one concludes that the AB Dor flare was approximately 40 - 80 times stronger than the solar SOLSTICE flare.

Mariska *et al.* (1989) have made interesting hydrodynamical computations of impulsive flares (see also Mariska & Poland 1985). Their results are relevant to explain the main features of our flare at day 14.22, particularly the short time scale of the event. The model assumes that the impulsive phase of the flare is due to the heating and subsequent evaporation of the stellar surface by an energetic electron beam accelerated (by reconnection) at the apex of a coronal loop. During the beaming the chromosphere is heated and changed to a high density transition region. Initially the CIV 1549 line is formed in typical TR-conditions (electron densities 10^{10} cm^{-3}) but during the flare its formation density is rising to 10^{12} cm^{-3} . Impulsive high temperature lines (like CIV) are radiated from this collisionally heated plasma together with a hard X-ray pulse (Bremsstrahlung). The maximum heating occurs around 10^5 K , i.e. where the CIV 1549 line is formed.

The reference model of Mariska *et al.* (1989) can be scaled to reproduce the main characteristics of the day 14.22 flare, although one can not prove that the flare was exactly similar to the model. The electron beam flux was increased in the computations linearly in 30 s to $5 \times 10^{10} \text{ ergs cm}^{-2} \text{ s}^{-1}$ and after that in 30 s decreased to zero again. The hardness of the electron beam was characterized by the low energy cut-off 15 keV and spectral power

law index $\delta = 6$. However, the results of Mariska et al. were quite insensitive on the choice of δ ($\delta=4$ gave practically the same results). Most important parameters were the injection flux and the time scale.

Ten seconds after the beginning of the heating the differential emission measure at 10^5 K increased to 10^{48} cm^{-3} , assuming (in the models) a flaring loop with 3000 km cross section (the hydrodynamics itself is completely independent of this selection). If the cross sectional area would have been 1900 - 3800 times larger, the observed AB Dor flare maximum differential emission measure $10^{51.3-51.6}$ cm^{-3} could be achieved. This means 0.5 - 1.0 % flare coverage of the total stellar surface.

Using the Mariska *et al.* electron flux parameters one can estimate the total number of injected electrons as $10^{39.9-40.2}$ during the flare at day 14.22 (by integrating over the electron injection time and energy profiles, eqs. 9 and 10 in Mariska *et al.*). At typical coronal loop electron densities (10^{10} cm^{-3}) this amount of electrons is already existing in a reservoir volume of $10^{29.9-30.2}$ cm^3 (before the reconnection). For the loop foot point radius estimated above ($(0.65 - 0.92) \times 10^{10}$ cm = $(0.09 - 0.12) \times R_{\odot}$) this means a $(0.06 - 0.17) \times R_{\odot}$ long piece of a flux tube as the reservoir of the injected electrons, e.g. at the apex of an already existing coronal loop.

EDITOR: PLACE FIGURE 6 HERE.

4. Bimodal Line Profiles. Narrow and Broad Components.

The accumulated quiescent profile of the CIV doublet (with flares extracted and shown in Fig. 6) can be fitted with four Gaussians (at the non-rotating stellar surface), broadened with the 90 km s^{-1} rotational (Gray function) and 15 km s^{-1} instrumental (Gaussian)

profiles (narrow and broad components at each line of the CIV doublet). In this way we have assumed that the transition region lies close to the photosphere, which is the case for normal coronal loops. However, it is possible that AB Dor has a co-rotating 'extended' transition region with a larger rotation velocity which may explain the width of the narrow component.

The linear limb darkening coefficient was assumed to be zero (no darkening nor brightening). The results were found to be quite insensitive to this choice. Moving the coefficient between +1 and -1, produced only 5 per cent changes in the intrinsic FWHM-values.

The mean fitting parameters (radial velocity relative to the stellar surface, FWHM, flux at the stellar surface and differential emission measure) for the whole doublet are presented in Table 3. 30 km s^{-1} was used as the radial velocity of the star itself (Vilhu *et al.* 1987). The narrow and broad components have roughly equal fluxes in AB Dor and both indicate large non-thermal velocities, much larger than the 15 km s^{-1} thermal velocity of CIV at 10^5 K .

5. Discussion

Using low resolution X-ray spectroscopy with the *Einstein* and *Exosat*, coronae of active stars were best fitted by two thermal components with temperatures around $(3-7) \times 10^6$ and $(2-5) \times 10^7 \text{ K}$, respectively, with varying relative emission measures (e.g. Swank *et al.* 1981; Schmitt *et al.* 1990; Lemen *et al.* 1989), although the reality of this bimodality is somewhat in doubt. If the coronal gas is fitted with one single (mean) temperature, a clear correlation between the temperature and activity level exists (Gagne *et al.* 1995). In the 2-T models the relative strength of the hot component rises with the CIV flux intensity

(Vilhu & Linsky 1990). A similar trend was found by Gagne *et al.* in the Pleiades: the coronal mean temperature clearly correlated with L_X/L_{bol} .

Using ASCA, White *et al.* (1996) fitted the quiescent spectrum of AB Dor with a 2-T plasma (7×10^6 K and 1.7×10^7 K) with roughly equal emission measures for both components. Combining the EUVE spectrum with that of ASCA (Mewe *et al.* 1996) gives best fits for 7.2×10^6 K and 1.9×10^7 K with emission measures 9.0 and 6.5 (in units of 10^{52} cm $^{-3}$), respectively (for the iron abundance $0.32 \times$ solar value). We found roughly equal emission measures for the narrow and broad components of CIV. Hence, it is tempting to speculate that the two velocity fields we see in the CIV-profiles of AB Dor are related to separate velocity field regions at the bases of two coronal patterns, hot and cool. However, multitemperature fits are also possible as demonstrated by Dupree *et al.* (1993) for Capella, using EUVE.

No trace of this bimodality or extra non-rotational broadening can be seen in the nearby chromospheric SiII 1533.4 line, nor in the earlier observations of photospheric absorption lines. This supports the idea that the broadening is related to motions in the transition region only. However, the MgII 2800 k and h resonance lines are somewhat broader than expected from the rotational broadening only. Rucinski (1985), using the IUE, found $\text{FWHM} = 159 \pm 4$ km s $^{-1}$ and $= 150 \pm 4$ km s $^{-1}$ for the k and h lines, respectively. At the line bases the total widths were 289 ± 9 km s $^{-1}$ and 232 ± 9 km s $^{-1}$ corresponding to rotational velocities $v \sin i = 142 - 116$ km s $^{-1}$. Since the instrumental profile of the IUE high resolution spectrograph at 2800 Å was around 20–30 km s $^{-1}$, some non-thermal velocities might be present but not so large as observed in the CIV 1550 lines.

Linsky *et al.* (1995) and Wood *et al.* (1997) proposed that microflaring (solar explosive events type phenomena) is behind the broad component. However, there is another possible hypothetical mechanism to explain the broad component (observed Gaussian $\text{FWHM} =$

330 km s⁻¹) we see in the quiescent spectrum of Fig. 6. Suppose that this component is not arising in large X-ray loop structures at all, but within the slingshot prominence complexes we see in H α , discovered by Collier Cameron & Robinson (1989). The co-rotating slingshot prominence system we see transiting the disc of AB Dor is concentrated around 2.7 to 3 stellar radii from the rotational axis (where the centrifugal force equals the gravity). This gives each individual cloud a velocity half-amplitude of 270 km s⁻¹. A large enough number of these could well mimic a Gaussian with FWHM in the required range. However, this mechanism is highly speculative since we have no physical model to explain why the prominence system should contain 10⁵ K gas. Hence, the physics behind the broad component is likely to be real microflaring (solar explosive events type microflares) as suggested by Linsky and collaborators.

To explain the broadening of the narrow component (FWHM = 68 \pm 2 km s⁻¹, including the 15 km s⁻¹ thermal broadening), it is tempting to look also at the Sun. Dere & Mason (1993) fitted the average solar CIV-profile with a non-thermal component with FWHM = 27 \pm 5 km s⁻¹. Adding the thermal broadening, a total FWHM = 42 \pm 5 km s⁻¹ results. Alternatively, they could fit the profile with two Gaussians (FWHM = 33 km s⁻¹ and 66 km s⁻¹, with relative intensities 1:2).

Random multiple velocities as seen in the high spatial and spectral resolution CIV Spacelab-data by Brynildsen et al (1995) are probably the physical reason for this extra non-thermal broadening of the narrow component. We co-added these Spacelab-data spatial pixels and the average line profile could be well fitted with a Gaussian profile with FWHM = 39 \pm 5 km s⁻¹ (the Spacelab data by Brynildsen, private comm.), confirming the result by Dere and Mason. The same broadening was obtained for both a quiet and an active region, which was somewhat a surprise.

However, this need not to be the final word. One can still speculate about extended

transition regions and slingshot prominences as sources for these broadenings, at least in the case of AB Dor.

6. Conclusions

We observed AB Doradus with the GHRS spectrograph of the *Hubble Space Telescope* on November 14.08 - 14.30, 1994 (UT). The medium resolution grating G160M was used with time and spectral resolution of 27 s and 15 km s⁻¹, respectively (post-COSTAR). The wavelength band observed (1531 - 1565 Å) included the strong CIV doublet (1548.202 and 1550.774 Å, formed in the transition region at 10⁵ K), the weak chromospheric SiII 1533.432 line and a blend of SiI, CI and FeII lines at 1561 Å. The following main results were obtained:

1. The quiescent state of AB Dor (see Table 3) is characterized by the CIV surface flux $F_{CIV} = (7.80 \pm 0.34) \times 10^5$ ergs cm⁻² s⁻¹. This is almost the same as the “saturated” value at K0-2 spectral type (8×10^5 ergs cm⁻² s⁻¹, see Vilhu 1987). The quiescent CIV 1549 line profile of AB Dor is bimodal and was fitted with two Gaussian profiles (narrow and broad), after the rotational and instrumental profiles were removed. The best fits were (for the line centroid radial velocity minus the stellar radial velocity 30 km s⁻¹, FWHM and total surface flux): NARROW (8 ± 1 km s⁻¹, 68 ± 2 km s⁻¹, $4.00 \pm 0.16 \times 10^5$ ergs cm⁻² s⁻¹) and BROAD (2 ± 4 km s⁻¹, 334 ± 8 km s⁻¹, $3.80 \pm 0.18 \times 10^5$ ergs cm⁻² s⁻¹). The bimodal structure of the quiescent CIV line profile might be due to two different broadening mechanisms and velocity fields at 10⁵ K. The width of the narrow component can be due to solar type TR transient events (random multiple velocities, but with a much higher filling factor), while the broad component could arise from frequent microflaring. The possibility that the broad line component comes from a ring of sling-shot prominences at 2 - 3 stellar radii, deserves to be further studied.

2. The transition region of AB Dor (as seen in the CIV line emission) is flaring frequently in different time scales and magnitudes (see Figs. 3 and 4). The quiescent mean flux was $f_{CIV} = (1.19 \pm 0.05) \times 10^{-12}$ ergs cm⁻² s⁻¹ on the Earth. The variability over the whole observing run is characterized by the standard deviation $1\sigma = 5.4 \times 10^{-13}$ ergs cm⁻² s⁻¹, while the 1σ of the individual data points in the light curve (Fig. 4) equals to 1.6×10^{-13} ergs cm⁻² s⁻¹. This means that the star spends about 15 per cent of time outside the 3σ -level from the quiescent state. It is even possible that the quiescent state itself is composed of many overlapping microflares, as suggested by the broad line component. The chromospheric lines (SIII 1533.432 and the blend of SiI, CI and FeII lines at 1561 Å) remained constant within a 3σ -level.

3. The largest impulsive flare seen in the CIV 1550 emission at day 14.22 reached in less than a minute the differential emission measure of $10^{51.2}$ cm⁻³ ($= N_e^2 V$ between $10^{4.85}$ K - $10^{5.15}$ K) and returned to the 7 times lower quiescent level after 5 minutes (see Table 2). During the flare peak the surface flux (on the star) reached the value of $F_{CIV} = (5.13 \pm 0.20) \times 10^6$ ergs cm⁻² s⁻¹. The total energy of the flare radiated in the CIV 1549 line was $1.65 \pm 0.10 \times 10^{31}$ ergs. The profile of the line during this flare (3 min average) was modelled with the quiescent profile *plus* a broad (FWHM = 800 km s⁻¹) and blue-shifted (-190 km s⁻¹) Gaussian. During the flare, slightly blue-shifted (-50 km s⁻¹) and narrow (FWHM = 55 km s⁻¹) absorptions appeared, having equivalent widths of 0.3 Å and 0.2 Å in the 1548 and 1550 Å lines, respectively (after the quiescent profile was subtracted).

4. The impulsive transition region flare at day 14.22 can be qualitatively understood with the help of the hydrodynamical models by Mariska *et al.* (1989), based on similar time scales of the event and the models. In this comparison the flaring loop foot point area covered (0.5 - 1.0) % of the total stellar surface. The total number of injected electrons can be estimated around 10^{40} needing a reservoir of a volume of 10^{30} cm³ at the apex of a

typical coronal loop (the reconnection area).

We thank Dr David Soderblom for the assistance to study the wavelength scale of GHRS and Drs Jeffrey L. Linsky and Thomas R. Ayres, the referees, for valuable comments and criticism. We are grateful to Prof. P. Maltby and Dr. N. Brynildsen for making available Spacelab solar data.

REFERENCES

- Brekke B., Rottman G.J., Fontenla J. & Judge P.G. 1996, ApJ, 468, 418.
- Brueckner G.E., Bartoe J.-D.F., Cook J.W., Dere K.P., Socker D., Kurokawa H. & McCabe M. 1988, ApJ, 335, 986.
- Brynildsen N., Kjeldseth-Moe O. & Maltby P. 1995, ApJ455, L81
- Cameron A.C. & Robinson R.D. 1989, MNRAS, 238, 657
- Dere K.P., Bartoe J.-D. and Brueckner G.E. 1989, Sol. Phys., 123, 41.
- Dere K.P. & Mason H.E. 1993, Sol. Phys., 144, 217
- Dupree, A., Brickhouse N.S., Doschek G.A., Green J.C. & Raymond J.C. 1993, ApJ, 418, L41.
- Gagne M., Caillault J.-P. & Stauffer J. 1995 ApJ, 450, 217
- Guirado J.C. et al. (22 authors) 1997, ApJ, December.
- Innis J.L., Thompson K., Coates D.W., Lloyd Evans T. 1988, MNRAS, 235, 1422.
- Lemen J.R., Mewe R., Schrijver C.J. & Fludra A. 1989, ApJ, 341, 474
- Linsky J.L. & Wood B.E. 1994, ApJ, 430, 342
- Linsky J.L., Wood B.E., Judge P., Brown A., Andrusis C. & Ayres T.R. 1995, ApJ, 442, 381
- Mariska J.T. & Poland A.I. 1985, Sol. Phys., 96, 317
- Mariska J.T., Emslie A.G. & Lie P. 1989, ApJ, 341, 1067
- Mewe R., Kaastra J.S., White S.M. & Pallavicini R. 1996, 9th Cambridge Workshop on 'Cool stars, Stellar systems and the Sun', R. Pallavicini and A.K. Dupree (eds.), ASP Conf. Series, 109, 273.

- Norris J.P., Nemiroff R.J., Davis S.P., Kouveliotou C., Fishman G.J., Meegan C.A. & Paciesas W.S. 1994, AIP Conference Proceedings on 'Gamma-Ray Bursts', G.J. Fishman, J.J. Brainerd & K. Hurley (eds.), 307, 172.
- Rucinski S.M. 1985, MNRAS 215, 591
- Rucinski S.M., Mewe R., Kaastra J.S., Vilhu O. & White S.M. 1995, ApJ, 449, 900
- Schmitt J.H., Collura A., Sciortino S., Vaiana G.S., Hardnen F.R. Jr & Rosner R. 1990, ApJ, 365, 704
- Swank J.H., White N.E., Holt S.S. & Becker R.H. 1981, ApJ, 246, 208
- Vilhu O., Tsuru T., Collier Cameron A., Budding E., Banks T., Slee B., Ehrenfreund P. & Foing B.H. 1993, A&A, 278, 467
- Vilhu O. 1987, in J.L. Linsky and R.E. Stencel (eds.) 'Cool Stars, Stellar Systems, and the Sun', Lecture Notes in Physics No. 291, Springer-Verlag, p.110
- Vilhu O. & Linsky J.L. 1990, Adv. Space Res. Vol 10 (No.2), p.139
- Vilhu O., Muhli P., Huovelin J., Rucinski S.M., Collier Cameron A., Slee B., Budding E., Banks T., Foing B. & Tsuru T. 1996, 9th Cambridge workshop on 'Cool stars, Stellar systems and the Sun', R. Pallavicini and A.K. Dupree (eds.), ASP Conf. Series, 109, 297.
- White S.M., Pallavicini R. & Lim J. 1996, preprint.
- Wood B.E., Harper G.M., Linsky J.L. & Dempsey R.C. 1996, ApJ, 458, 761.
- Wood B.E., Linsky J.L. and Ayres T.R. 1997, ApJ, 478,745.

Fig. 1.— The time-averaged spectrum of AB Doradus taken with the GHRS of the Space Telescope using the grating G160M.

Fig. 2.— The optical U-band light curve of AB Dor during the present *HST* observations covering the day fraction 0.08 - 0.30, corresponding to rotational phases 0.21 - 0.64 (Eq. 1). A photospheric dark spot region seen face-on at phase 0.5 is responsible for the minimum.

Fig. 3.— The dynamic spectrum of AB Dor at the CIV 1549 doublet. The time goes vertically upwards (total 5.5 hours) and the wavelength increases from left to right. The impulsive flare at day 14.22 discussed in Ch. 3 is seen as the brightest horizontal spike.

Fig. 4.— The light curve of the total CIV 1549 doublet with 27 s binning.

Fig. 5.— The CIV light curve around the strongest flares. The model fits are included (Eq. 2). (a) Day 14.185 flare. Seconds are counted from the day fraction 14.173. (b) Day 14.22 flare. Seconds are counted from the day fraction 14.207.

Fig. 6.— Spectra of AB Dor at CIV 1549 during the strongest flare and the quiescent state. Upper: The time averaged (exp = 3 min) flare spectrum at day 14.22 Nov 1994, with 4-Gaussian fits (the dashed lines). Lower: The quiescent spectrum accumulated during 150 minutes of observation with flaring extracted. The intrinsic (non-rotating) 4-Gaussian components (dashed lines) were further broadened with the 90 km s⁻¹ rotational and 15 km s⁻¹ instrumental profiles to obtain the best fit shown by the solid line (difficult to see against the stellar spectrum). Note that the flaring narrow component is almost identical to the quiescent profile. The continuum is shifted by 5.0 and -4.0 (10⁻¹³) for the flare and quiescent spectra, respectively.

AB DORADUS AVERAGE SPECTRUM HST/GHRS/G160M

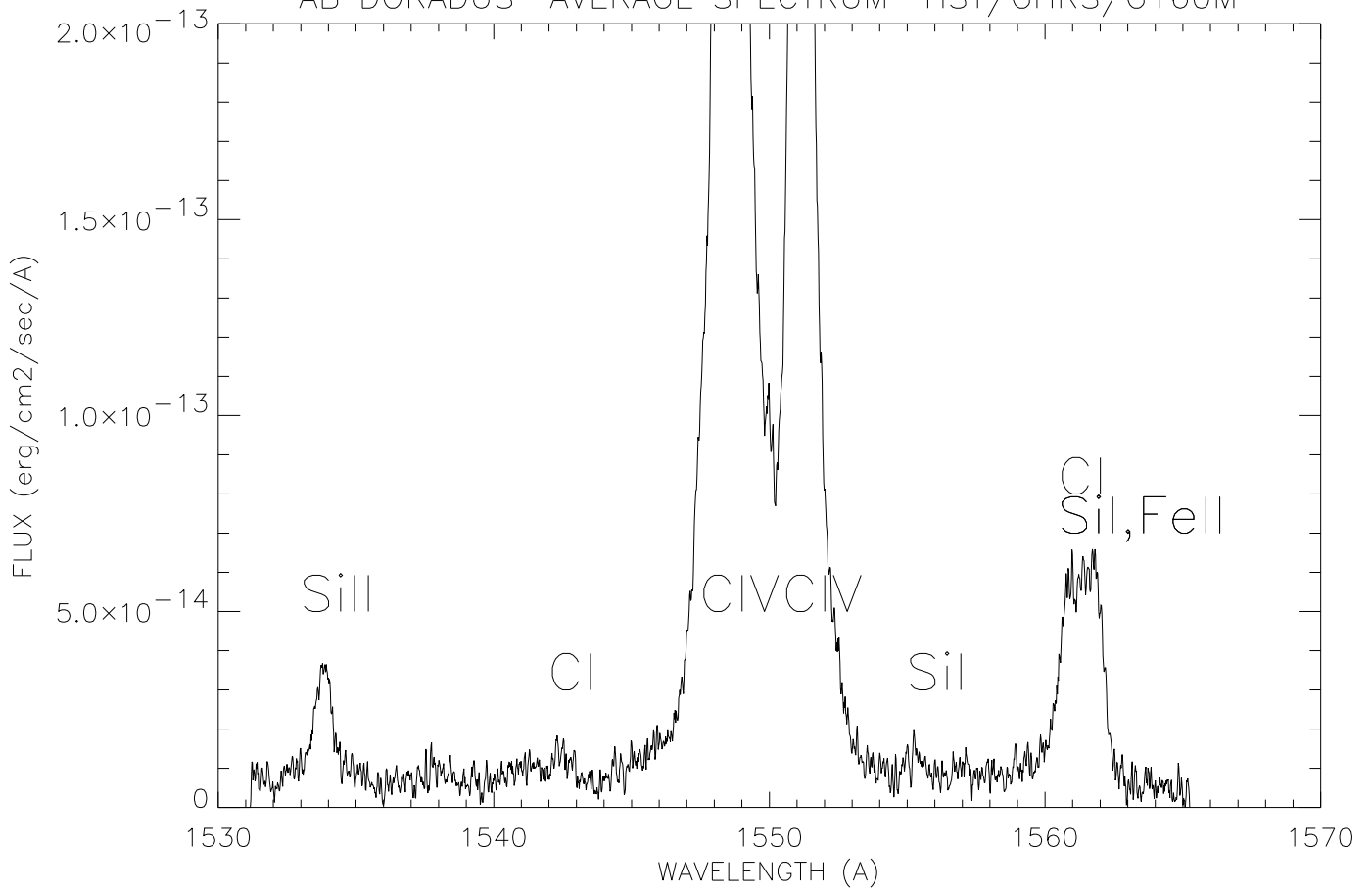


TABLE 1. Observations of AB Doradus with the HST/GHRS.

DATE (UT)	GRATING	WL-RANGE	RES. POWER	TIME RES.
November 14.08 - 14.30, 1994	G160M	1531 - 1565 Å	20000	27 sec

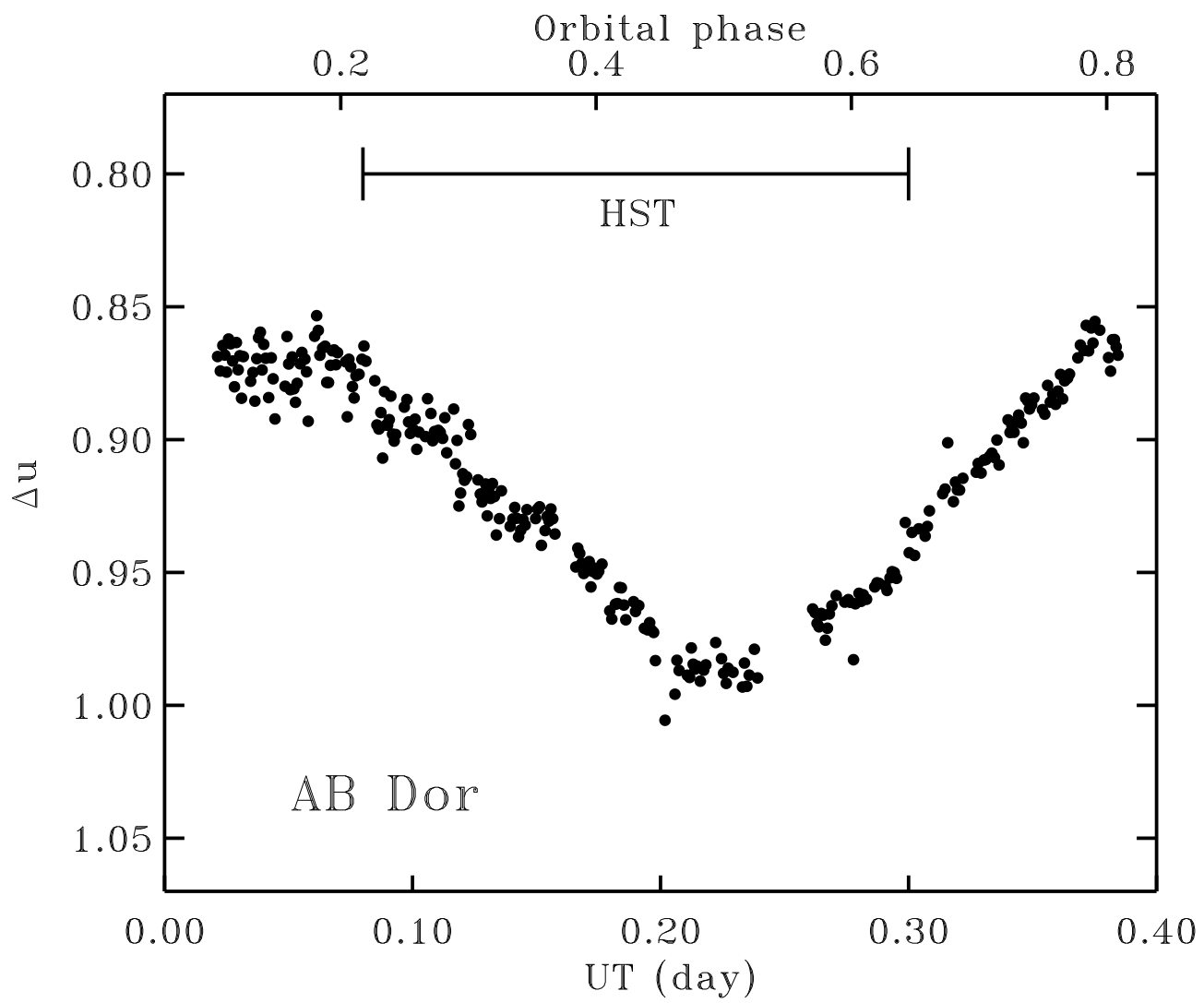


TABLE 2. Derived parameters for the CIV 1550 line of AB Dor during the day 14.22 flare ^a

rise time σ_r ^b	decay time σ_d ^b	peak time t_{max} ^b	peakedness ν ^b	V_{rad} ^c	FWHM	$F_{CIV}(\max)$ ^d	$\log(\text{DEM}(\max))$ ^{d,e}	$E(\text{tot})$ ^d
s	s	UT		km s ⁻¹	km s ⁻¹	$\times 10^6$ ergs cm ⁻² s ⁻¹	cm ⁻³	$\times 10^{31}$ ergs
26±4 :	96±17	14.2179±0.0000	0.94±0.14	-190±20	800±50	5.13±0.20	51.20±0.02	1.65±0.10

^aCIV 1548.202 and CIV 1550.774. 3 min average line profiles, quiescent part subtracted. Instrumental (15 km s⁻¹) and rotational (90 km s⁻¹) profiles extracted. Based on data from the HST/GHRS/G160M observing run on November 14.08 - 14.30, 1994 (UT).

^bBy fitting the CIV lightcurve (27 s time resolution) with Eq. (2).

^cRelative to the star. $V_{rad}(\text{star}) = 30$ km s⁻¹.

^dUsing $d = 15$ pc.

^eDEM = the differential emission measure between $\log T = 4.85$ – 5.15

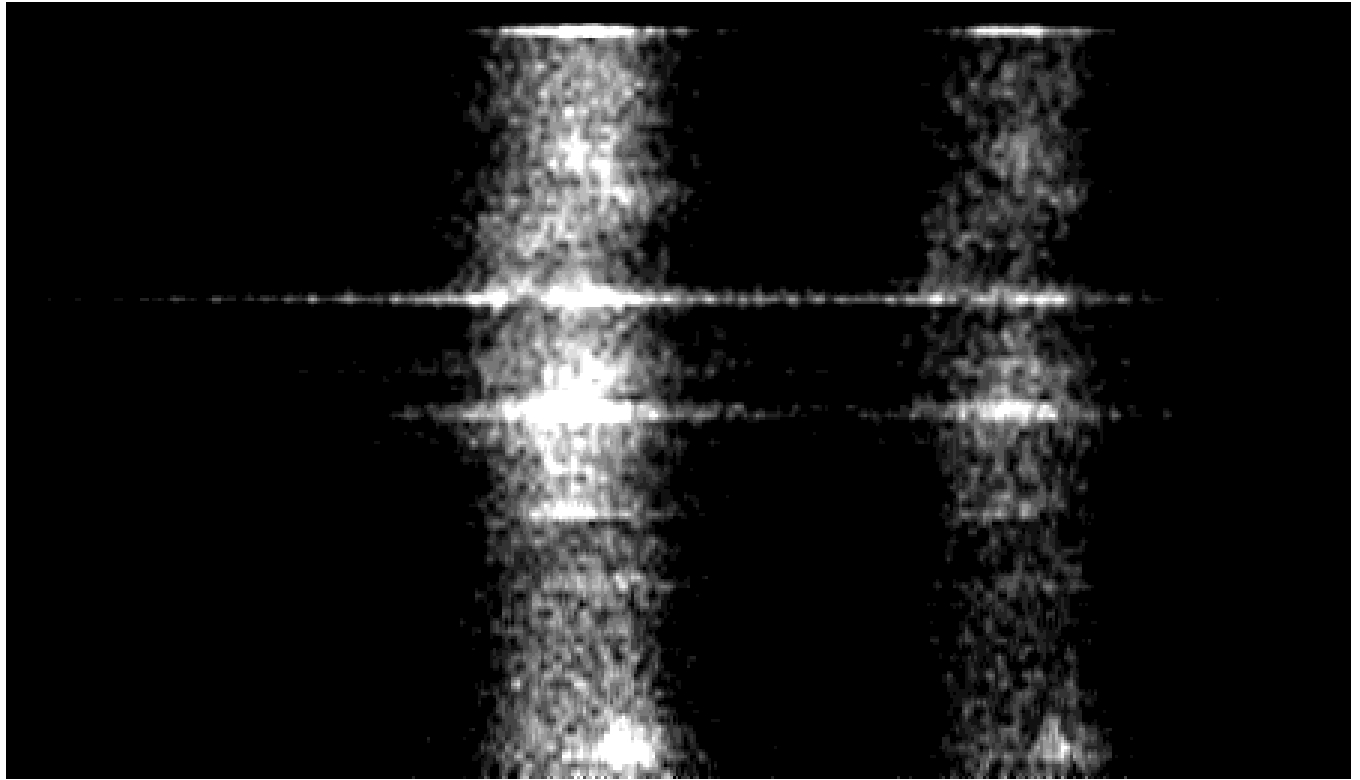


TABLE 3. Derived parameters for the CIV 1550 line of AB Dor in quiescence. ^a

Component ^b	V_{rad} ^c km s ⁻¹	FWHM km s ⁻¹	F_{CIV} ^d $\times 10^5$ ergs cm ⁻² s ⁻¹	log(DEM) ^{d,e} cm ⁻³
NARROW	8±1	68±2	4.00±0.16	50.09±0.02
BROAD	2±4	334±8	3.80±0.18	50.07±0.02

^aCIV 1548.202 and CIV 1550.774. Instrumental (15 km s⁻¹) and rotational (90 km s⁻¹) profiles extracted. Based on data from the HST/GHRS/G160M observing run on November 14.08 - 14.30, 1994 (UT).

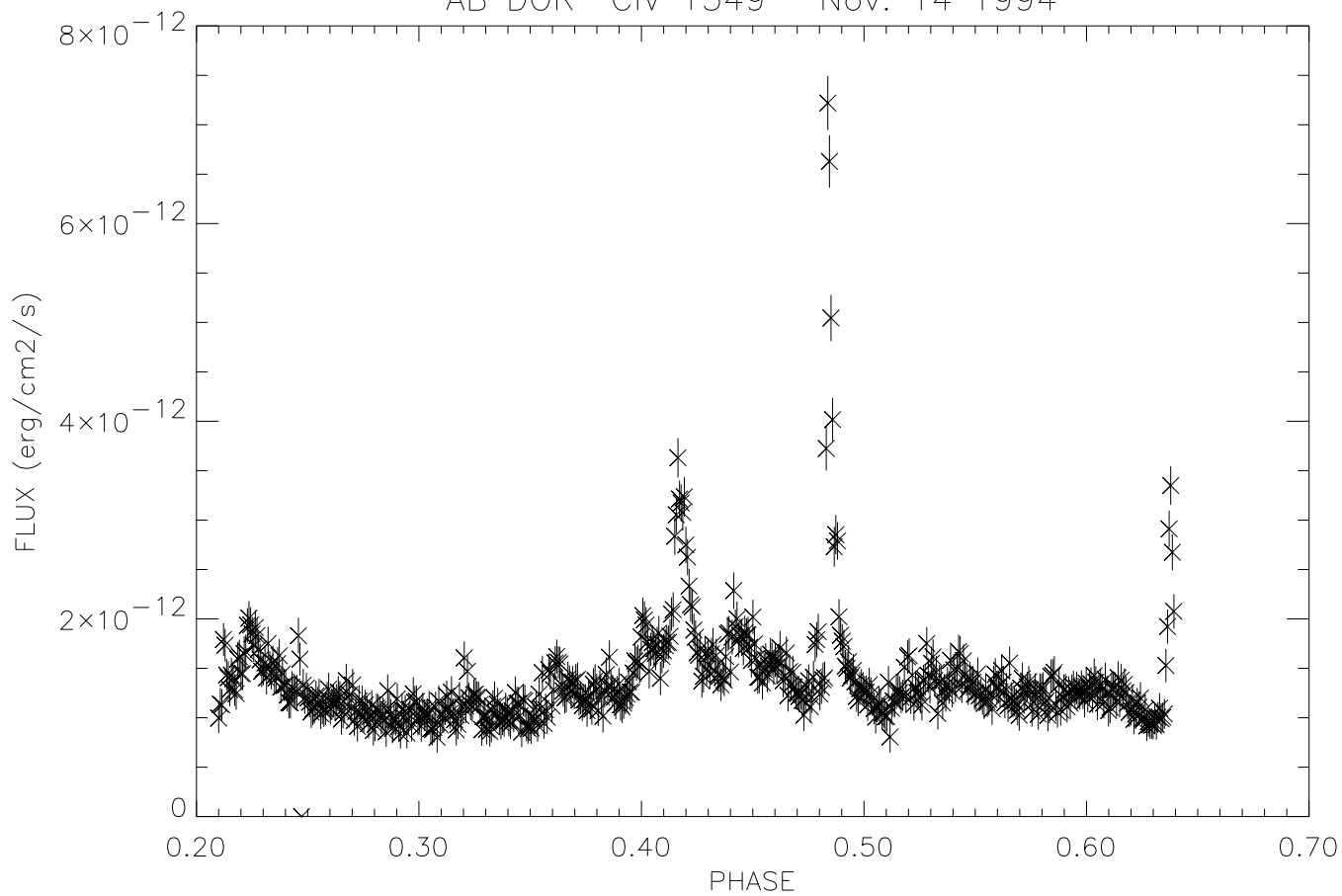
^b2-Gaussian fit to the line profile.

^cRelative to the stellar surface. $V_{rad}(\text{star}) = 30$ km s⁻¹.

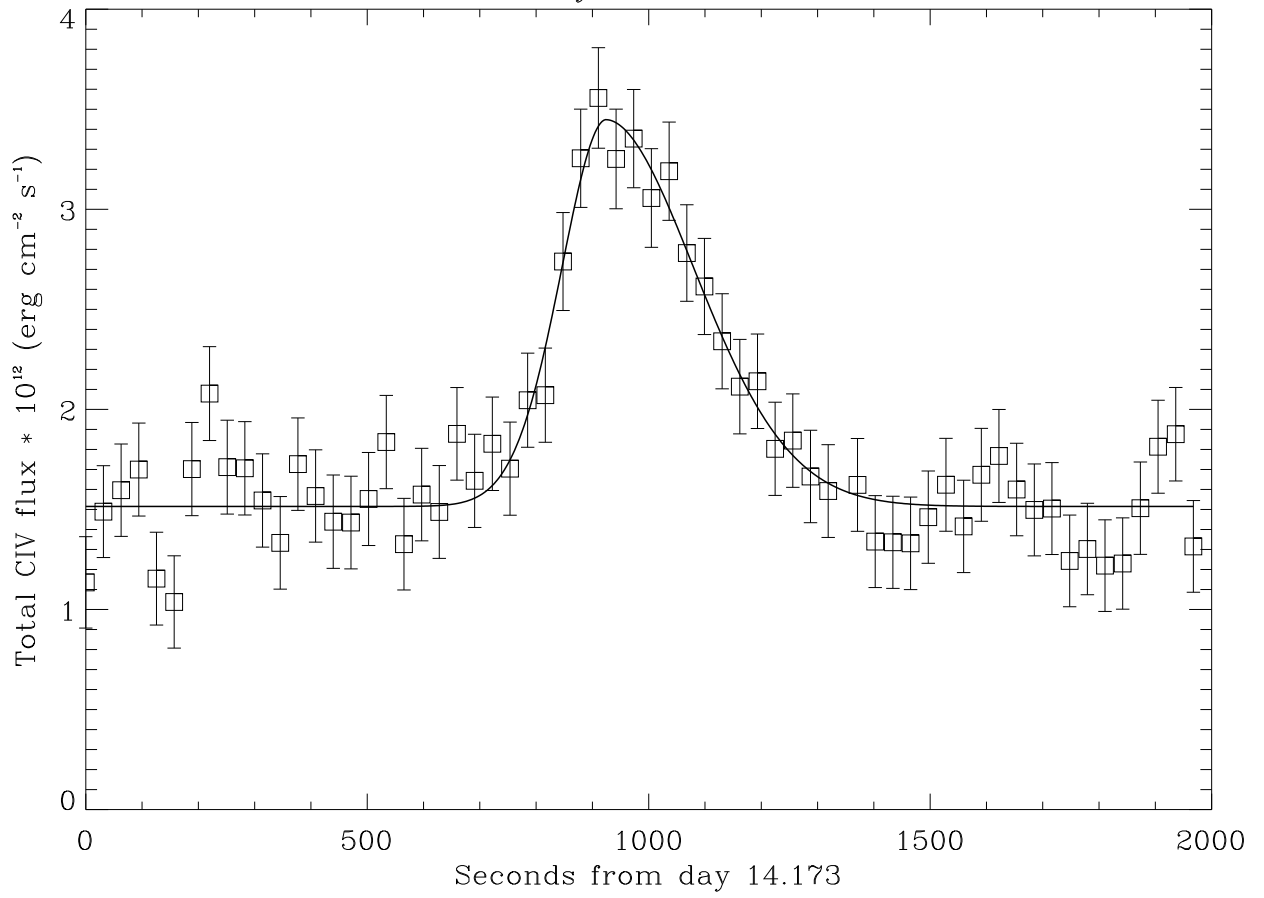
^dUsing $d = 15$ pc.

^eDEM = the differential emission measure between $\log T = 4.85$ – 5.15 .

AB DOR CIV 1549 Nov. 14 1994



CIV doublet flux at the day 14.185 flare + fit to GRB model



CIV doublet flux at the day 14.22 flare + fit to GRB model

